Characterizing Disorder in the Electrostatic Potential Landscape of Quantum Dot Devices

Zeest Fatima

Presented as partial fulfillment of the requirements of PHYS 437 B.

Department of Physics and Astronomy

University of Waterloo

Canada

April 2nd, 2024

Table of Contents

Introduction:

Quantum dot (QD) devices leverage the spin degree of freedom of electrons to function as qubits. Spin is a fundamental property of nature and serves as an excellent qubit because it naturally provides a two-level system that is largely insensitive to electric fields, resulting in long quantum coherence times. Quantum dot devices trap and confine electrons (in potential wells) by manipulating the electrostatic potential landscape of the device, using voltage electrodes as gates. A well-controlled potential landscape of the device is thus very important for the confinement of the electrons. One of the greatest challenges in the scalability of silicon-based quantum dot devices is the variation in electron-transport characteristics of functionally identical devices, due to randomly distributed charge defects and material imperfections in the device [10]. Furthermore, these defects also affect the electrostatic potential landscape of the device, causing there to now be a disordered potential landscape, or “disordered potentials”.

There have already been various attempts to infer the disordered potential landscape of the device (due to charge defects in silicon), using electron transport measurements such as Scanning Gate Microscopy (SGM) [3,4]. Though these techniques are useful for better understanding the disordered potentials, transport measurements become less feasible as systems scale up in size. Thus, for this project, we decided to investigate whether non-transport-based qubit characterization measurements could be useful in providing information about the device’s disordered potential landscape.

Furthermore, simulations were used to study the various kinds of qubit characterization measurements, since not only do simulations grant us access to a much larger volume of data, but also because they enable us access to quantities that may not be directly experimentally accessible. For example, if we can quantify how disorder in the electrostatic potential landscape affects various parameters of the Hamiltonian of the system (specifically, the Hubbard Hamiltonian, which is not directly experimentally accessible), we can get an idea of how the disorder could be inferred from charge stability diagrams, which are experimentally accessible, as well as directly correlated with the Hubbard Hamiltonian's parameters.

Brief overview of what was done during Phys 437A

For Phys 437A, we tried to find correlations between the density and spatial position of charge defects, and parameters of the Hubbard Hamiltonian (i.e Hubbard parameters) as well as the "G-factor" (which is based on the quadratic stark shift). The order of operations was as follows:

1) We simulated our silicon-based double quantum dot device with various configurations of manually placed charge defects.

   The various defect scenarios differed by the z-plane the defects were placed in, the number of defects placed, as well as their distribution in the x-y plane. I.e for a specific z-plane value, as well as for a fixed number of defects placed, there were various configurations of random distribution of defects in the x-y plane.

2) What was simulated for these various configurations was the electrostatic potential landscape.

3) For each of the simulated potential landscapes, we extracted Hubbard parameters, as well as looked at the G-factor deviations.
4) We then used a supervised machine learning model (specifically, Support Vector Machine (SVM)) to evaluate whether either of the Hubbard parameters and g-factor values were strongly correlated with the density and z-plane of charge defects.

Results:

- There wasn't a notable correlation between the g-factor deviation with either the defect z-plane or the number of defects.
- For Hubbard parameters, they had a strong correlation with some specific defect densities. I.e. for the five density values we tested (number of defects ranging from 20 to 40, at intervals of 5), the machine learning model was able to predict three out of five of those defect densities using the Hubbard parameters, with precision ranging from 70% to 90%.

Plan outline for Phys 437B

Instead of trying to find correlation between multiple quantities at once, we decided to focus on the correlation between the spatial location of the defects and the six Hubbard parameters. More specifically the goals for this term were as follows:

1) On the quantum dot device, superimpose a 3x3 grid. Then at the center of each of the boxes of the grid, place a single defect one by one.
2) Simulate the potential landscape of the grid for each defect configuration.
3) For each defect configuration, extract the six Hubbard parameters.

4) For each configuration, write the Hubbard parameters as components of a vector, so that now each disorder configuration has an associated 6 dimensional vector, with components being the Hubbard parameters.
5) Analyze components of the vectors relative to each other, to look for correlation between Hubbard parameters and spatial position of charge defects in the x-y plane.

Overview of gate defined quantum dot devices

Semiconductor spin qubits rely on three-dimensional confinement of electrons. See Fig. 1 for a cross-sectional view of the device. The confinement in the z-direction is done using a semiconductor heterostructure, while confinement in the x-y plane is done using voltage gates, which create potential wells in the electrostatic potential landscape of the device, and trap electrons in those wells. A semiconductor heterostructure is a material made by joining two or more different semiconductors with varying properties, such as bandgap, lattice constant, or doping levels. The heterostructure can, for instance, be made of layers of Silicon (Si) and Silicon Oxide (SiO_2) stacked together. Furthermore, when specific voltages are applied to the voltage gates, electrons accumulate in between the Si and SiO_2 layers, forming a layer of electrons called the 2-Dimensional Electron Gas (2DEG) layer. [1]

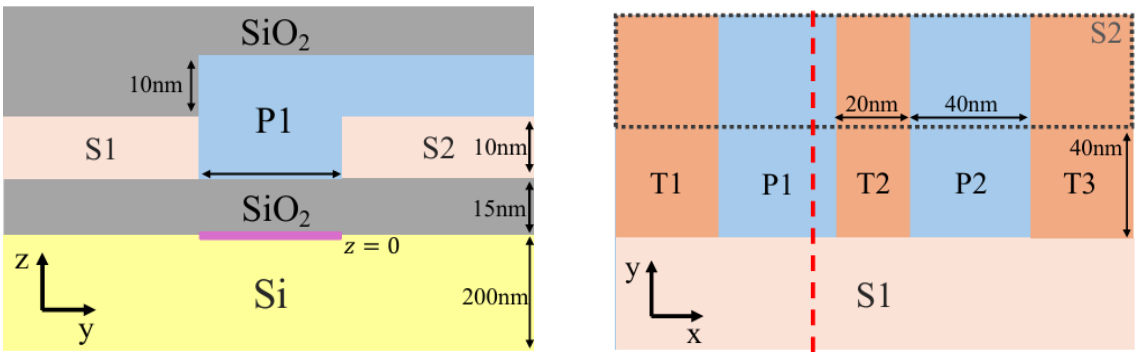

A **B**

Fig. 1 A: Cross-sectional view of our Si/SiO2 quantum dot device, through the red line drawn in **B**. P1 is the plunger gate, and S1 and S2 are screening gates. A layer of electrons accumulates between the Silicon and Silicon Oxide (SiO2) layer right below the plunger gate, called the 2-Dimensional Electron Gas (2DEG) (in pink). The plunger gate (blue) confines electrons (in the 2DEG) in the z-direction by forming a potential well. The trapped electrons form quantum dots. The screening gates are there to limit the effect of the plunger gate, so that the potential wells are only formed at a specific spot and the size of the dot is constrained. **B:** Top-view of the device. T1, T2 and T3 are tunnel barrier gates and P1 and P2 are plunger gates. The border of screening gate S2 is represented by the grey dotted line, indicating its position below the plunger and tunnel barrier gates. [10]

The device has 6 metallic gates, as shown in Fig 1. During regular operation, a positive voltage is applied to the two plunger gates, which causes electrons to accumulate in the 2DEG layer. The screening gates and the tunnel barrier gates are used for dot confinement, which they do by depleting the 2DEG from underneath them using lower voltages than plungers. The quantum

dots form under the unscreened portions of the plunger gates, and are usually 40 x 40nm large [10].

Gating and the Electrostatic Potential Landscape of the Device

The electrostatic potential created by the voltage gates can be quantified as a function of position in each of the x, y and z planes. Changes in gate voltages of either of the gates alter both the quantum dot's electrochemical potential, as well as the shape of the confining potential. If one were to model the confining potential in 3D, they would get a 3-dimensional parabola with the electrons confined at the minima. Furthermore, Quantum dots can be connected in series to make larger structures, such as the double quantum dot (DQD). In a DQD, there are two potential wells separated by a potential barrier. See Fig. 2 for a visualization of the potential landscape with two wells. Furthermore, the interdot barrier height can be voltage-controlled to modulate the interdot tunnel coupling. Usually there exist gates called tunnel and barrier gates which control the dot electrochemical potentials and interdot barriers, respectively. Furthermore, geometrical cross-capacitances between the dots influence the potential under neighboring gates.

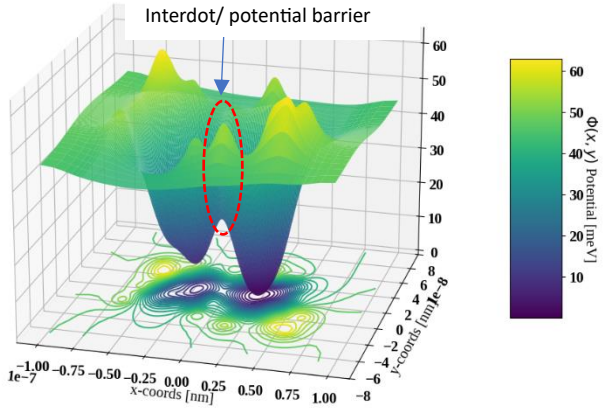

Fig. 2 Electrostatic potential landscape of a quantum dot device. The two wells form two separate quantum dots.

Electron-electron interactions:

Band structure and electrostatic confinement allow the formation of 0-dimensional quantum dot states, as well as the trapping of individual electrons (and hence spins). As more electrons are added to a quantum dot, the electron-electron Coulomb interaction becomes critical to the properties of the whole system. The coulomb interaction essentially refers to the repulsive force that the two electrons impose upon each other. So electrons trapped in a QD electrostatically repulse any other electron attempting to join that dot, which is also referred to as Coulomb Blockade. This classical effect defines the charging energy

$$E_C = e^2/C$$

where C is the total dot capacitance. In order to overcome the effects of coulomb blockade, a quantum dot system could be biased (referring to voltage biasing).

For a system with one quantum dot containing only one electron, the possible states the system could be in are an orbital ground state, and a first excited state. The two states are separated in energy by $E_{orbital}$. Then when a second electron is added to the dot, the spatial wavefunctions

must be either symmetric or antisymmetric under particle exchange, which correspond to spin singlet and triplet states, respectively. Singlet states can have both electrons occupy the same or different (spin-degenerate) orbitals, while triplet states must have electrons in separate orbitals, due to spatial anti-symmetry.

Restricting ourselves to the two lowest orbital states for simplicity, the ground state spin singlet comes from double occupation of the ground orbital, while the triplet states are higher in energy as they must place one electron each in the ground and first excited orbitals. In the absence of a magnetic field, the triplet states are degenerate with energy by E_T , and the singlet-triplet splitting is given by J where

$$J = E_T - E_S$$

is positive. This example illustrates the general principle that any two-electron system (even spanning multiple QDs) has a singlet ground state in the absence of magnetic fields.

As for the matter of detecting and measuring charges in the quantum dot (and hence the number of electrons trapped inside), quantum point contact can be used. Quantum Point Contact (QPC) detects the charge states of individual quantum dots by serving as a highly sensitive, tunable conductor. It operates as a narrow, quasi-one-dimensional channel in a 2DEG, where the conductance is quantified in units of

$$\frac{2e^2}{h}.$$

The presence or absence of a single electron in a nearby quantum dot modifies the electrostatic potential near the QPC, which affects its conductance. This provides a non-invasive way to measure the charge state of the quantum dot.

Capacitance model and Hubbard Hamiltonian:

Quantum dots with weak coupling between them and thus well localized charges separated from the remaining of the electron gas can be modelled by the Capacitance Model, also referred to as the Constant-Interaction Model. The Constant-Interaction Model is a classical description based on two assumptions: 1) the Coulomb interactions between electrons on dots and in reservoirs are parametrized by constant capacitances, and 2) the single-particle energy-level spectrum is considered independent of electron interactions and the number of electrons, meaning that quantum mechanical energy spacings are not taken into account. [2]

The Constant Capacitance Model however does not account for quantum effects, and thus is not the most accurate way to model the dynamics of a double dot system. Alternatively, there is the Hubbard model, which models it more accurately.

The Hubbard model can be written as a Hamiltonian in the following form:

$$\hat{\mathcal{H}} = -\sum_i \mu_i \hat{n}_i - \sum_{\langle i,j\rangle,\sigma} t_{ij}\left(\hat{c}^\dagger_{i\sigma}\hat{c}_{j\sigma} + \hat{c}^\dagger_{j\sigma}\hat{c}_{i\sigma}\right) + \sum_i \frac{U_i}{2}\hat{n}_i(\hat{n}_i - 1) + \sum_{i\neq j} U_{ij}\hat{n}_i\hat{n}_j,$$

Chemical potential term

Kinetic energy (i.e hopping) term

On-site interaction term

Long range interaction term

Fig. 3 Hubbard Hamiltonian and its various terms.

The chemical potential accounts for the effect of the chemical potential μ_i on each site i (where site could just mean each of the quantum dots). The chemical potential controls the energy cost or gain of adding a particle to site i, helping to maintain the desired particle number in the system. The kinetic energy, or hopping term on the other hand describes the motion of electrons between neighboring sites i and j. The hopping amplitude t_{ij} determines the probability of an electron with spin σ moving between sites. The on-site interaction term on the other hand models the repulsion between electrons occupying the same site. U_i quantifies the strength of this repulsive interaction. Since electrons are fermions and subject to the Pauli exclusion principle, this term becomes significant when two electrons with opposite spins occupy the same site. Finally, the long-range interaction term accounts for Coulomb interactions between electrons at different sites i and j. U_{ij} specifies the interaction strength between electrons at these sites. While typically smaller than the on-site interaction, it becomes important in systems where electrons are not well-screened, such as in extended or low-dimensional systems.

Now that we have talked about the specifics of the system, let us move on to what was done.

Disorder Model

Various types of defects can exist in the device, including interface traps, grain boundaries, dopants and magnetic dipoles [5,6,7]. Except for grain boundaries (static defects), the rest of the defects listed can be classified as two-level fluctuators (TLFs), which are further classified as either whole charge, dipole charge, or spin fluctuations [5]. The presence of TLFs results in qubit dephasing for both single-spin and spin-triplet qubits.[8] Based on the work done by

Culcer and Zimmermann [5], where they study the effects of various TLFs on dephasing times of singlet-triplet qubits, and conclude that whole-charge defects are typically more effective at dephasing singlet-triplet qubits compared to other defect classes, we chose to model the disorder in our device as spheres with fixed negative charge of 1*e*. Furthermore the spheres have a radius of 2nm and are modelled after a shallow donor in silicon [9].

Simulation Workflow and Calculating Hubbard Parameters

First using the nextnano simulation software, which is a Poisson-Schrodinger finite element method (FEM), we can simulate electrostatic potential landscapes of our double quantum dot device by defining the device's geometry as well as the disorder geometry. It takes in *.in* files for the input files, and generates nextnano output files, which then contain the potentials and information about the electric field. Furthermore for each voltage configuration of the 3 gates (T2, P1 and P2 from Fig 2.) that we vary in the system, a new nextnano file has to be run. For example, if we want to vary the two plunger gates from 0.2V to 0.4V and the tunnel barrier from −0.1V to 0.1V in steps of 0.1V, there would be 27 nextnano files that would need to be simulated. [10]

What was done was that previously written scripts (by Ali Sakr) were modified. The first script could create multiple iterations of nextnano files varying by defect density and z-plane position, and randomized charge placement, as well as varying this over the voltages described above (so that we would end up with a total of 27 files for each unique configuration of density, charge distribution and z value). It was modified so that now it was superimposing a 3x3 grid at a specific z-plane value (z=10nm, whereas keep in mind that the dots are formed at z=0 nm). Then

for each box in the grid, one by one, it would place a single charge of negative 1e in the center of each of the boxes, in only one box at a time. So we ended with 9 separate disorder configurations (see Fig 4). Then for each disorder configuration (where the “disorder” was placed at the center of the grid), we also generated 27 files, varying by the same gate voltages as described above. So in total we had 9 x 27 nextnano input files that the code generated, and then we ran those through nextnano to get potential landscapes for each of them.

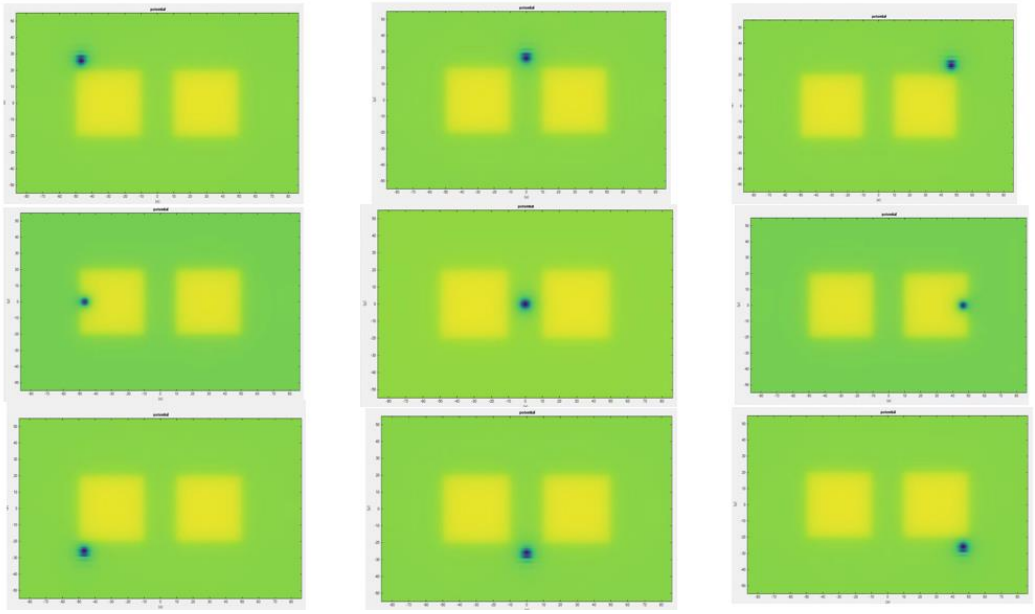

Fig 4. Potential in the x-y plane, taken from right below the plunger gates. The yellow squares are the plunger gates, and notice the dark green dots placed at various positions around them. Those are the charge defects, placed about 10 nm below the plunger gates.

Furthermore, when deciding on the value of fixed charge to be placed, spot checks were done that helped determine what the charge of the defect should be. -1e was determined to be the highest value of charge, since anything above that placed in the specific z-plane would alter the potential well a fair bit, and make it much harder to use the well at those voltages to confine the electrons (see figures 5, 6 and 7).

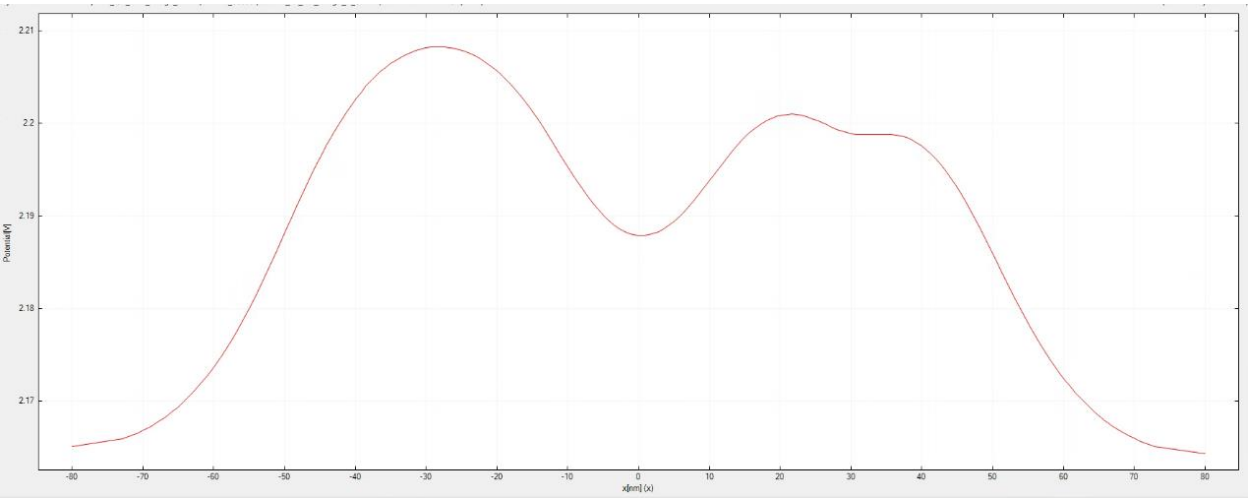

Fig 5. Plot of the potential in the x plane at y=0. These wells are upside down, since that is how nextnano displays them. But notice that the right well has a bump on it. This is due to a charge being placed right in the center of the right plunger gate (see Fig 7.). The charge placed here was -1e.

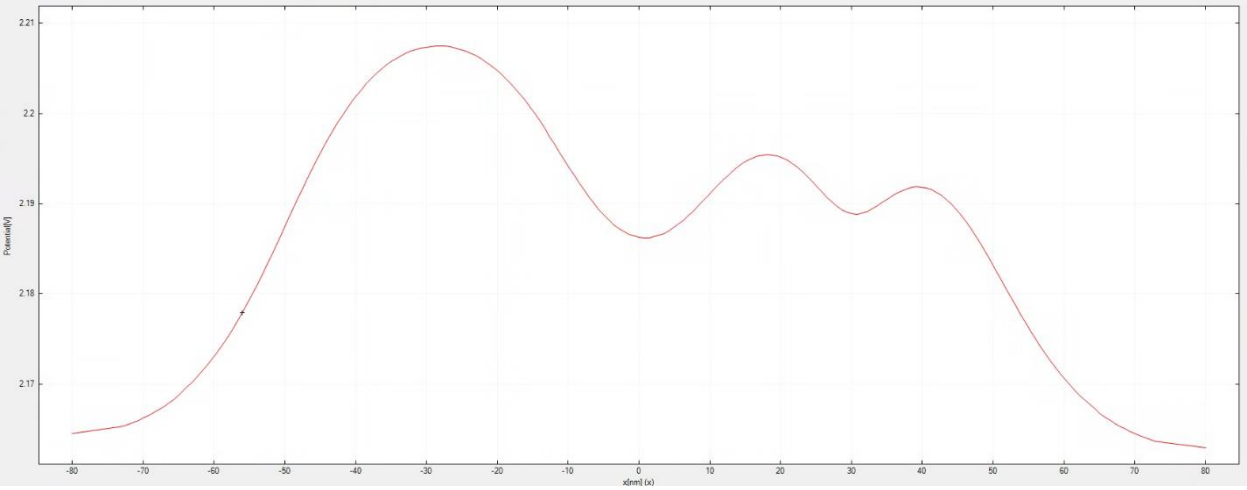

Fig 6. Identical to Fig. 5, except the charge placed now was -2e. Notice that one of the well shapes has already been distorted enough that it would be difficult to form a well confined quantum dot from it.

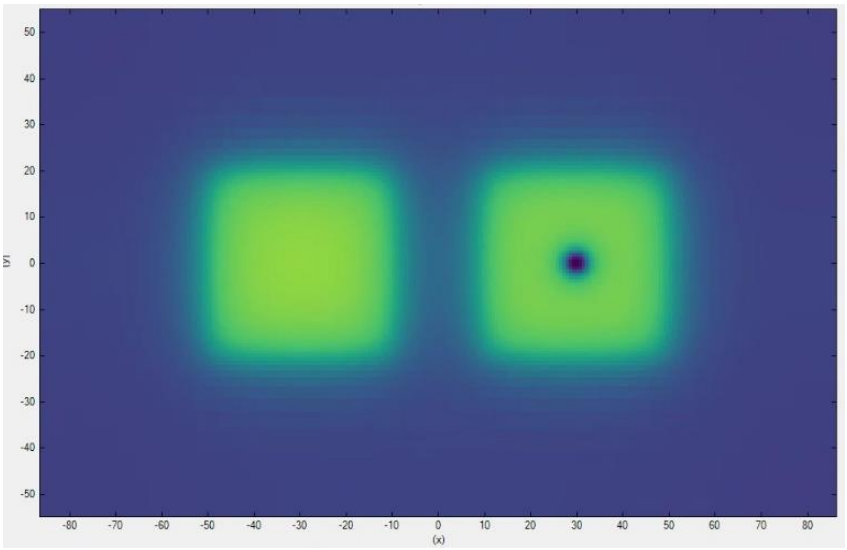

Fig 7. Placement of the charge for figures 5 and 6. Again note that the green boxes are the plunger gates, and the charge has been placed 10 nm below the gates. This image of the potential has been taken from the z-plane of the charge (z=10nm), and this is potential for that specific x-y plane.

Now talking about the simulation software that was used next, QuDiPy, i.e Quantum Dots in Python. QuDiPy is the Python-based quantum dot simulator being developed at the Baugh group. It can take in a group of nextnano output files as an input (with all the files corresponding to a single device and disorder configuration, and varying only by gate voltage configurations) and generate an interpolation object. This interpolation object is unique to a given disorder configuration, and essentially allows us to access the potential landscape at any gate voltage configuration within the bounds of those simulated in nextnano, where any voltage value that was not simulated in nextnano is linearly interpolated. [10] This has many benefits, one of which is allowing us to have a single object that refers to each disorder configuration, as opposed to multiple files. Additionally, QuDiPy interpolation objects take up much less storage space than nextnano output files, which is crucial when dealing with very large amounts of data

(i.e for 130 nextnano output files corresponding to storage space of 50GB, compared to the interpolation objects for those files being 700MB).

Using QuDiPy, first the interpolation objects were created. Then through two other QuDiPy scripts, Hubbard parameters were generated for each of the 9 disorder configurations. The scripts were written for the Phys 437A project by Ali Sakr, and were modified for the 3x3 grid case this term by me.

Here are some sample plots that were generated comparing the potential with no disorder, to the case with the charge defect placed in the (1,1) box in the 3x3 grid.

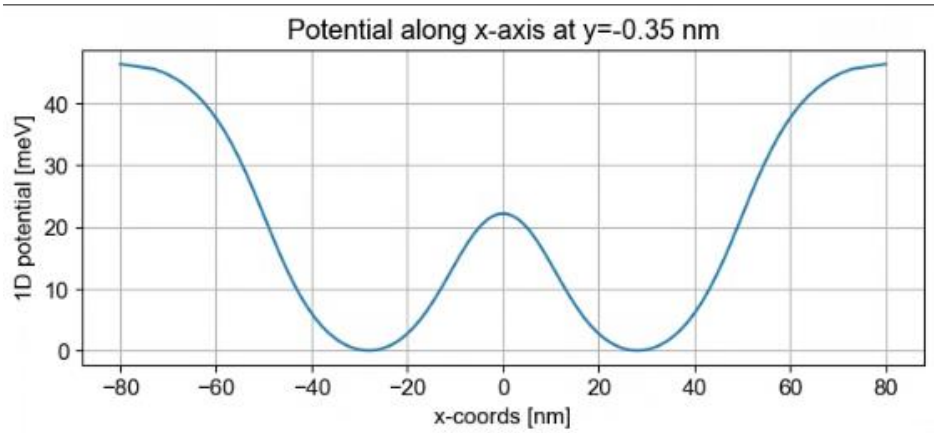

Fig 8. 1D potential in x at y=0 for the non-disordered case. Note the well minima are symmetrical.

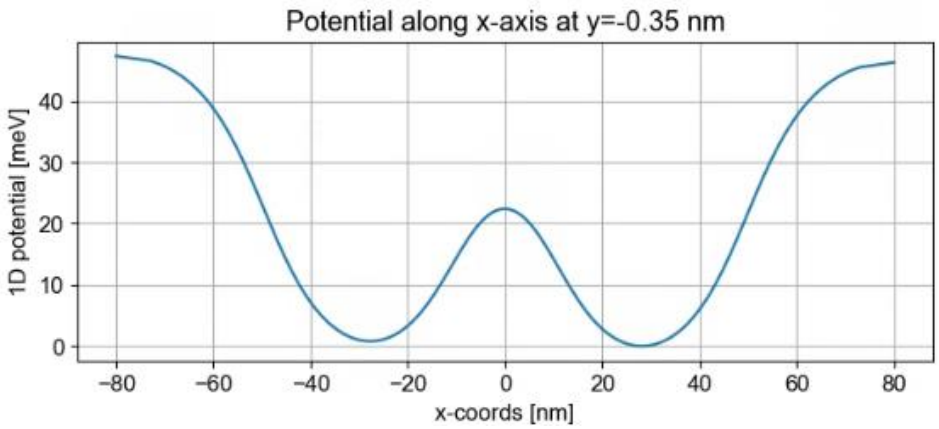

Fig 9. Same as Fig 8 but with disorder, with the defect placed in the (1,1) position (top left box in the 3x3 grid). Notice that the left well is slightly less deep at the minima compared to the right one.

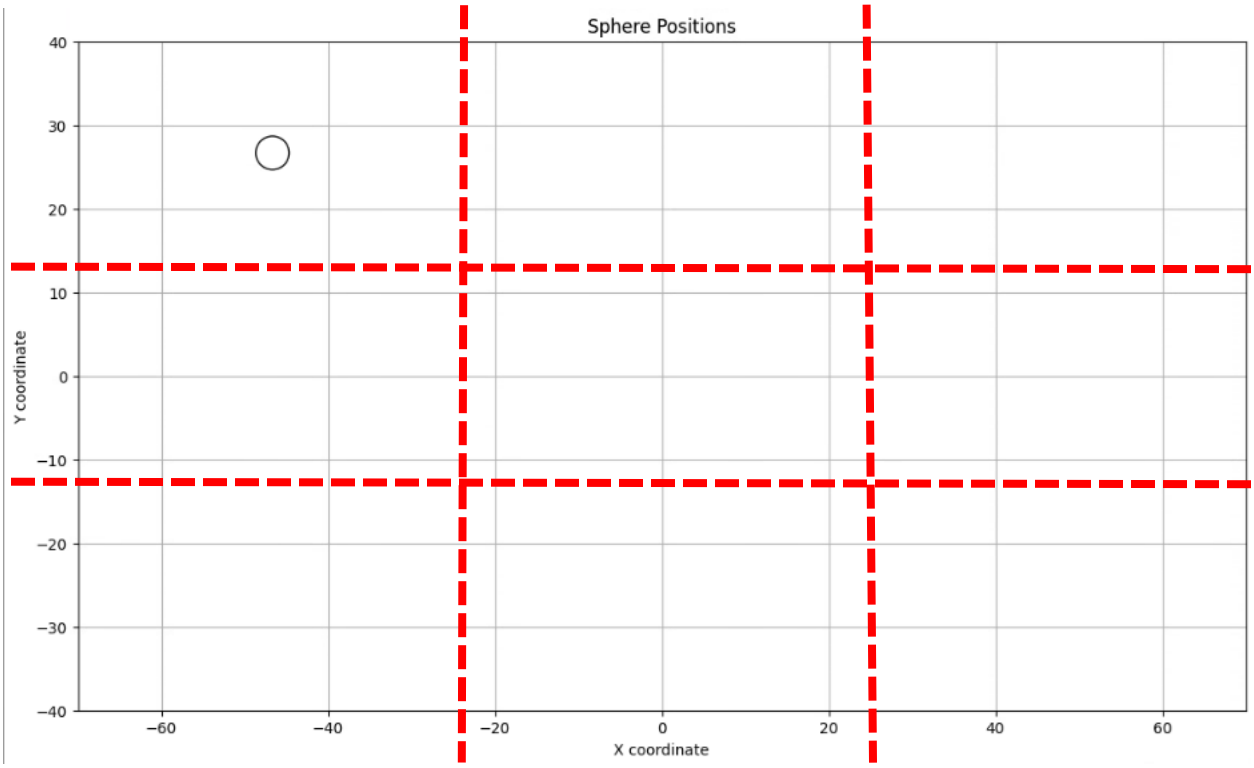

Fig 10. Sphere (charge) placement for the (1,1) case. The red dotted lines are approximately how the 3x3 grid is defined. The sphere is the charge.

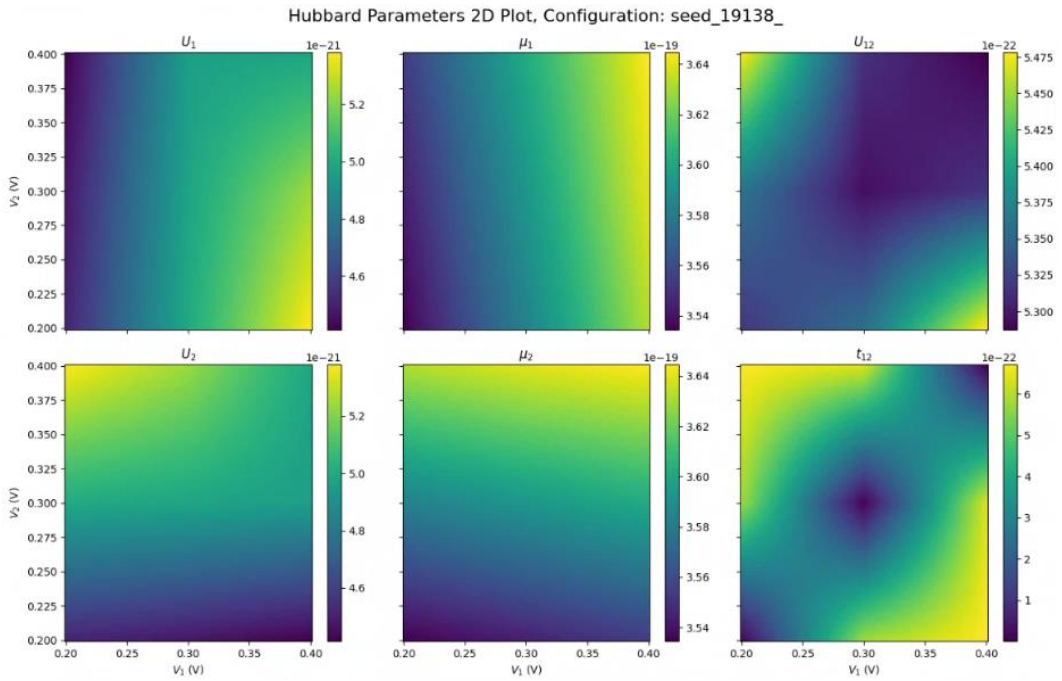

Fig 11. Hubbard parameters for the non-disordered case. 2D plot of the parameters plotted as a function of voltages for T2, P1 and P2.

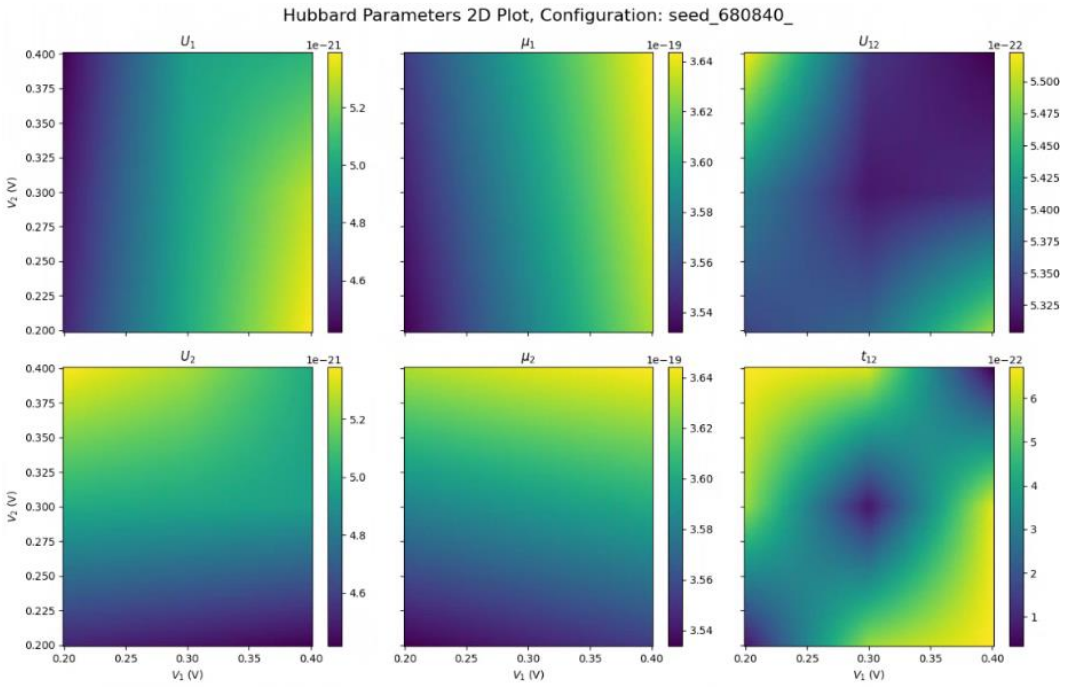

Fig 12. Hubbard parameters for the case where disorder was placed in the (1,1) grid box. 2D plot of the parameters plotted as a function of voltages for T2, P1 and P2.

Next Steps

So what was done so far this term was the simulation of the 9 disordered and non-disordered potential cases, as well as extraction of the Hubbard parameters. The next step would be to extract the Hubbard parameters at specific points in these voltage spaces, and writing them as components of a 6-dimensional vector. The vectors could then be analyzed through various techniques including calculating their Euclidean distances (which is just the Euclidean norm),

$$d(\vec{H}_i, \vec{H}_j) = \sqrt{\sum_{k=1}^{6} (H_{i,k} - H_{j,k})^2}$$

where *i* and *j* are components of the vectors. From this method we can build a heatmap of how much the parameters vary as a function of defect position. Another method could be calculating the Mahalanobis Distance, which would take into account correlations between Hubbard parameters and scale with their variances:

$$d(\vec{H}_i, \vec{H}_j) = \sqrt{(\vec{H}_i - \vec{H}_j)^T S^{-1} (\vec{H}_i - \vec{H}_j)}$$

where S is the covariance matrix of the Hubbard parameters across all defect positions.

Lastly, we can also use Cosine Similarity, which measures orientation instead of magnitude,

$$\cos(\theta) = \frac{\vec{H}_i \cdot \vec{H}_j}{\|\vec{H}_i\| \|\vec{H}_j\|}$$

which would tell us whether the "direction" of parameter change is similar between defect positions.

Acknowledgements

I would like to acknowledge first that that this work took place on the traditional territory of the Neutral, Anishinaabeg, and Haudenosaunee peoples. The UWaterloo campus is situated on the Haldimand Tract, the land granted to the Six Nations that includes six miles on each side of the Grand River.

Furthermore, I would like to acknowledge all the support I received from Prof. Jonathan Baugh during this project, as well as support from our visiting Masters student Ali Sakr last term, current Master's student Xinning Wang, and PhD student Zach Merino, as well as rest of the group members.

References

1. Burkard, G., Ladd, T. D., Pan, A., Nichol, J. M., & Petta, J. R. (2023). Semiconductor spin qubits. Reviews of Modern Physics, 95(2), 025003. Available at: https://doi.org/10.1103/RevModPhys.95.025003
2. Darulová, J. (2020). Automated Tuning of Gate-Defined Quantum Dots (Doctoral Thesis). ETH Zurich. Available at: https://doi.org/10.3929/ethz-b-000473107
3. Ga¨etan J. Percebois and Dietmar Weinmann. Deep neural networks for inverse problems in mesoscopic physics: Characterization of the disorder configuration from quantum transport properties. Physical Review B, 104(7), August 2021.
4. D.L. Craig, H. Moon, F. Fedele, D.T. Lennon, B. van Straaten, F. Vigneau, L.C. Camenzind, D.M. Zumb¨ uhl, G.A.D. Briggs, M.A. Osborne, D. Sejdinovic, and N. Ares. Bridging the reality gap in quantum devices with physics-aware machine learning. Physical Review X, 14(1), January 2024.
5. Dimitrie Culcer and Neil M. Zimmerman. Dephasing of si singlet-triplet qubits due to charge and spin defects. Applied Physics Letters, 102(23), June 2013.
6. Michael Shur. Physics of semiconductor devices. Prentice-Hall, Inc., USA, 1990.
7. D.M. Fleetwood and R.D. Schrimpf. Defects in Microelectronic Materials and Devices. CRC Press, 2008.
8. Marco Fanciulli. Electron Spin Resonance and Related Phenomena in Low-Dimensional Struc tures, volume 115. 01 2009.
9. Gabriela Herrero Saboya. Defects in silicon : revisiting theoretical frameworks to guide ab initio characterization. Theses, Universit´ e Paul Sabatier- Toulouse III, November 2020

10. Ali Sakr. Exploring the Feasibility of Disorder Potential Inference using Non-transport Simulations of Quantum Dot Qubits in Silicon. Internship manual, University of Twente and University of Waterloo, September – December 2024.